Artificial Life and Robotics (2020) 25:81–88
https://doi.org/10.1007/s10015-019-00568-4

ORIGINAL ARTICLE

A study of a gravity compensation system for the spacecraft prototype test by using multi-robot system

Ayana Nakayama[1] · Tomohiro Hirata[1] · Katsuyoshi Tsujita[1]

Received: 24 April 2019 / Accepted: 1 August 2019 / Published online: 29 October 2019

Abstract
In our research, we proposed a system using multi-robot as a gravity compensation system for a ground test of a spacecraft with a deployable structure. The advantage of the system is its low cost and versatility. When the robots support the beam at the nodes, we can expect to simulate the free vibration of the space structure using the proposed system under gravity. In this study, supporting a uniform, flexible beam with vibration was first implemented to verify the performance of the proposed system. Then we investigated the performance of the system applying to the mock-up model of a spacecraft with a deployable structure as a demonstration.

Keywords Deployable space structure · Prototype test · Gravity compensation · Multi-robot

1 Introduction

In the field of space engineering, we encounter a new horizon of technology, such as deep space exploring, huge scale or tiny scale satellites, complex deployable structures, and so on. The hardware prototype test is an indispensable process in the development of the spacecraft [1–5]. The prototype test of deployment of space structures, such as large scape antenna, solar panels, membrane structures require gravity compensation during the structure's deployment motion on the ground. But, we cannot completely cancel the gravitational effects on the space structures on the ground, in principle. Therefore, the ground prototype tests need to be effectively implemented for each test issue, individually [6, 7]. The purpose of our research is to develop a prototype test system for deployable membrane or flexible space structures [8–13] using a multi-robot supporting system.

During the past twenty years, to support the deployment motion of spacecraft flexible structure, passive or actively controlled multi-point suspension systems have been developed [14–16]. There are two types of such gravity compensation systems. One is the suspension system, which has huge multi-point suspension with wires from the ceiling of the test facility [17]. The system needs to assign the supporting points discretely and, therefore, the dynamics of suspension wires affecting to the deployable mechanism of the spacecraft cannot be neglected. The other type of gravity compensation system utilizes weight supporting mechanisms such as air bearings [18]. The system well simulates the frictionless environment. But it requires a huge surface plate for the prototype test of a large spacecraft. In addition, the use of the system is restricted in the prototype test of two-dimensional deployment of space structure. Furthermore, the air bearing system has large inertia that may disturb the spacecraft's deployment dynamics. Therefore, it is difficult to apply these systems for the prototype test of inflatable structures or the three-dimensional deployable structures.

In our research, we proposed a support system using a multi-robot as a gravity compensation for ground prototype test of spacecraft with a deployable structure. If we use a multi-robot supporting system, all the robot have the same control architecture and do not need spacecraft-specific controller design. Therefore, we only have to change the number of the robot if the design of the spacecraft changes. The advantage of the system is its low cost and versatility. The system is expected applicable in the prototype test for various types of spacecraft, such as small satellites, huge

This work was presented in part at the 24th International Symposium on Artificial Life and Robotics, Beppu, Oita, January 23–25, 2019.

✉ Katsuyoshi Tsujita
e1316077@st.oit.ac.jp

[1] Department of Electrical and Electronic Systems Engineering, Osaka Institute of Technology, 16-5, Omiya 5, Asahi-ku, Osaka 535-8585, Japan

flexible space structures with many degrees of freedom. It can be established by changing the number of multi-robots according to the test conditions. The modular architecture and the portability of the robots reduce the cost of the system to set up the prototype test facility. In the previous study, we proposed a model of a lower-supported robot system and confirmed that it has a good support function in the deployment test of a simple deployment structure [19].

In general, lower-order modes, especially the first mode of the space structure, is a significant mode. Because the mode often leads to the critical situation of the space structure, such as unexpected deformation, damage to the structure, and so on [20]. Therefore, we focused on the first mode of the structure in this study. At first, we considered emulating the behavior of a uniform beam in the zero-gravity space for simplicity. The first mode of the simple beam vibration has two nodes under the free–free boundary condition. When the robots support the beam at the nodes, we can expect to emulate the free vibration of the space structure using the proposed system under gravity. In this study, supporting a uniform, flexible beam with vibration (i.e. the theoretical behavior is well known) was implemented to verify the performance of the proposed system, first. Then we investigated the performance of the system applying to the mock-up model of a spacecraft with a deployable structure as a demonstration.

2 System architecture

We propose a robotic gravity compensation system of the spacecraft prototype tests. The system is designed to emulate the friction-free environment in the space. The system is composed of some robots. The robots cooperatively support the structure of the spacecraft. The number of robots depends on the size or complexity of the spacecraft structure. Figure 1 shows the schematic architecture of the system. Each robot can be equipped with a mobile machine to move around the ground, according to the wide area deployment of the spacecraft. But in this article, we do not explain the mobile mechanism in detail, because the purpose of this study is to investigate the supporting conditions of the system for the target structure as a simple beam.

Each robot has six DOF (degrees of freedom) HEXA type parallel mechanism (Fig. 2). This mechanism enables to support and to guide the deployment of the target structure. The mechanism will cancel the load of the structure and emulate the friction-free environment, that is, space without external force. In the real environment in space, the structure of the spacecraft will cause a free vibration. The robot needs to emulate such special motion of the spacecraft.

3 Control system

The proposed control system is realized with a force controller of each robotic unit. The force controller enables gravity compensation to support the load of the target structure. It also follows the deployment motion or vibration of the target structure. The controller detects reaction forces at the supporting point and moves the traveling plate of the robot to cancel such forces. In this study, the controller was implemented by a simple PI force control. Receiving the force sensor signals, the controller generates the commanded linear velocity of the traveling plate, which compensates the reaction forces. According to the commanded motion of the traveling plate, joint angles of the parallel link mechanism

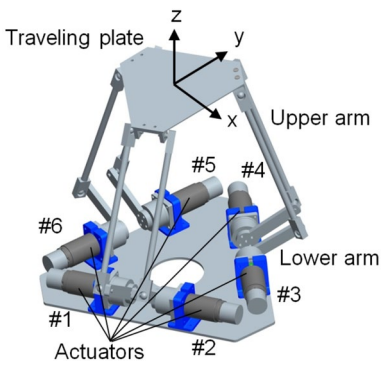

Fig. 2 Schematic model of the robotic unit

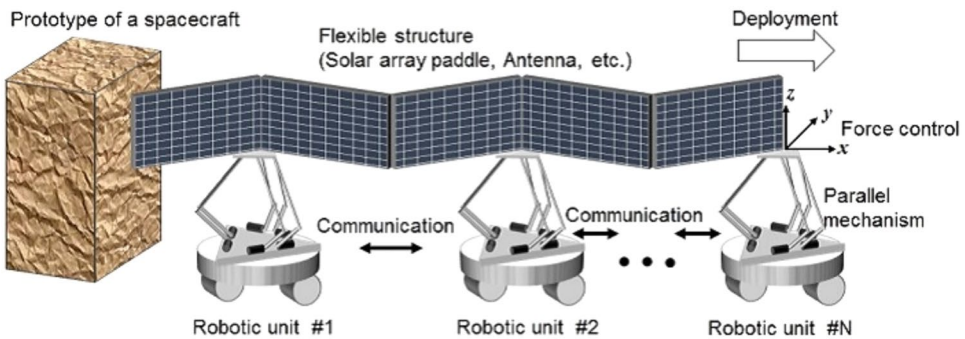

Fig. 1 System architecture

are calculated by inverse kinematics. A high gain PD feedback controller moves actuators for the traveling plate to coincide with the commanded motion.

First, the commanded value of the linear velocity of the traveling plate $\dot{X}_e^d = \left[\dot{x}_e^d, \dot{y}_e^d, \dot{z}_e^d\right]^{\mathrm{T}}$ is designed as follows:

$$\dot{X}_e^{(i)d} = K_{Pf}^{(i)}\eta^{(i)} + K_{If}^{(i)}\int \eta^{(i)}\mathrm{d}t - K_{Df}^{(i)}\dot{X}_e^{(i)} \tag{1}$$

$$\eta^{(i)} = \begin{bmatrix} -F_{sx}^{(i)} \\ -F_{sy}^{(i)} \\ F_{dz}^{(i)} - F_{sz}^{(i)} \end{bmatrix} \tag{2}$$

where $K_{Pf}^{(i)}, K_{If}^{(i)}, K_{Df}^{(i)}$ $(i = 1, \cdots, N)$ and N are feedback gain matrices, the number of modular robotic units, respectively. $F_{sx}^{(i)}, F_{sy}^{(i)}, F_{sz}^{(i)}$ are the measured value of the force sensor in x, y, and z-axes, respectively. $F_{dz}^{(i)}$ is the desired value of reaction force to compensate the gravitational force acting on the supporting point. The commanded value of angular velocity $\dot{\theta}_j^d$ (j: index number of the parallel link) for each actuator of the parallel link manipulator is calculated by the inverse kinematics.

$$\theta_j^{(i)d} = F\left(X_e^{(i)d}\right) \tag{3}$$

The actuator torque is controlled by high gain PD feedback as follows:

$$\tau_j^{(i)} = k_{Pj}^{(i)}\left(\theta_j^{(i)d} - \theta_j^{(i)}\right) - k_{Dj}^{(i)}\dot{\theta}_j^{(i)} \tag{4}$$

3.1 Feedback gains

With the traveling plate position vector as $X_e = [x_e, y_e, z_e]^{\mathrm{T}}$, the equation of motion is expressed as follows.

$$M\ddot{X}_e^{(i)} + C\dot{X}_e^{(i)} = Q^{(i)} \tag{5}$$

When the movement amount $|X|$ of the traveling plate is sufficiently smaller than the link lengths in Eq. (5), the driving force vector Q of the traveling plate is obtained using the motor torque vector $\tau_j^{(i)}$ of Eq. (4) can be approximated as follows.

$$Q^{(i)} = K_P'\left(X_e^{(i)d} - X_e^{(i)}\right) - K_D'\dot{X}_e^{(i)} \tag{6}$$

The shearing force Fs at the supporting point of the flexible structure is opposite in direction to the supporting reaction force at the supporting point and can be modeled as follows.

$$F_s^{(i)} = -kX_e^{(i)} = -Q^{(i)} \tag{7}$$

Table 1 Parameters of the parallel link manipulator

Diameter of the base unit	194 mm
Length of the lower link	65 mm
Length of the upper link	165 mm
Typical height of the supporting point	230 mm

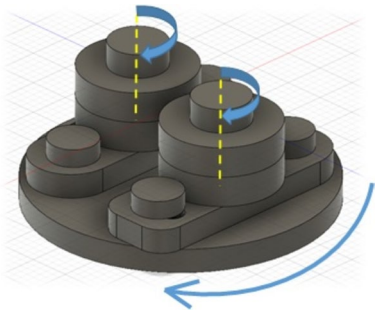

Fig. 3 Support jig on the top of the force sensor

From Eqs. (1), (5), (6), (7), the following equation is obtained.

$$\frac{\mathrm{d}^4}{\mathrm{d}t^4}X_e^{(i)} + \frac{K_D' + C}{M}\frac{\mathrm{d}^3}{\mathrm{d}t^3}X_e^{(i)} + \frac{K_P'\left(1 + K_{Df}^{(i)}\right)}{M}\frac{\mathrm{d}^2}{dt^2}X_e^{(i)} + \frac{K_P'K_{Pf}^{(i)}k}{M}\frac{\mathrm{d}}{\mathrm{d}t}X_e^{(i)} + \frac{K_P'K_{If}^{(i)}k}{M}X_e^{(i)} \tag{8}$$

Based on Eq. (8), the feedback gains are determined using the Routh–Hurwitz stability criterion so the system as to be stable.

4 Simultion model

4.1 Model of the robotic unit

Numerical simulations were implemented with the proposed system model. Table 1 shows the parameters of the robots.

Figure 3 shows the support mechanism which is mounted at the top of the force sensor, which clamps the target structure with two rotatable cylinders from both sides of the structure. The base plate to hold the two cylinders can be also rotatable. This mechanism is expected to follow the rotating motion of the supporting structure passively.

4.2 Simple beam model for the flexible structure

Consider a uniform beam whose length and the cross-sectional areas are l and A, respectively. First, we define y-axis in the longitudinal direction of the beam. Beam's elastic

deformation $x(y, t)$ is defined as a function of axial position y and time t.

$$\rho A \frac{\partial^2 x}{\partial t^2} + EI \frac{\partial^4 x}{\partial y^4} = 0 \tag{9}$$

The natural frequency and the shape function of the beam's vibration are derived as follows:

$$f_n = \frac{1}{2\pi} \left(\frac{m_n^2}{l^2} \right) \sqrt{\frac{EI}{\rho A}} \tag{10}$$

In this paper, we focused on two types of boundary conditions.

- Free-free: No shearing force nor bending moment at both ends of the beam.
- Both ends simply supported (B.E.S.S.): The beam is simply supported at two positions with shearing force without bending moment.

Shape functions according to the boundary conditions are illustrated in Fig. 4.

Here, we have to note that the vibration nodes are located at the points of 22% from both ends in terms of the first mode of free-free condition. It is well known that the first vibration mode of the structure is dominant in the zero-gravity environment and sometimes causes serious damage to the structure. In this paper, we considered the behavior of the first mode of free-free condition. Therefore, the supporting points of the proposed robotic system were located at the nodes of the first mode of free-free condition.

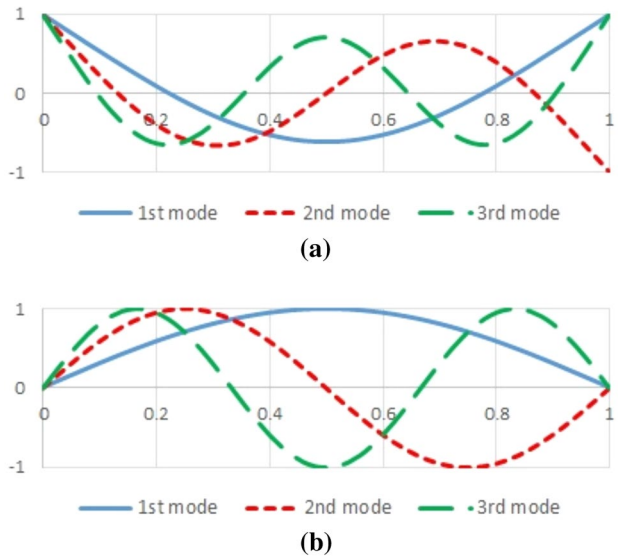

Fig. 4 Shape functions according to the boundary conditions

5 Numerical simulations

To verify the suitable supporting position of the robotic units, numerical simulations were implemented. Figure 5 shows the configuration of the simulation model.

Theoretical vibration modes of the beam could be analytically derived. The beam was made of stainless steel and the property of the beam was summarized in Table 2.

Using Eq. (10), the natural frequency of the first mode of the free-free condition is derived as 3.91 Hz. First, the uniform beam was modeled as a finite element model. The model was composed of a series connection of 100 rigid elements. The elements were connected through rotational joints. The joints had one rotational degree of freedom with elastic and viscous components. The elasticity and viscosity were set corresponding to the hardware setup based on preliminary experiments. Observing the profile of attenuation of vibration, the vibration when using the proposed control system is more attenuated than the free vibration under zero gravity. As an initial condition, 1 N of the external force in the direction perpendicular to the axis of the beam for 0.01 s.

Figure 6 shows the time history of the displacement at the geometric center of the beam and the frequency characteristic in the case of the free-free condition (zero gravity) and the case of using the proposed control system. From this result, 3.91 Hz, which is the frequency of the first mode in the case of free oscillation, has been observed in both cases, and by supporting the beam using the proposed control system, it is possible to preserve the original vibration mode. It can be seen that the free vibration under zero gravity can be appropriately

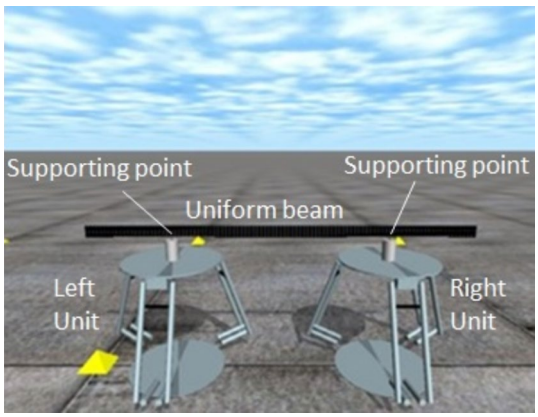

Fig. 5 A snapshot of the numerical simulation (two points simply supported condition)

Table 2 The property of the beam

Young's modulus	Thickness	Height	Length
197 GPa	9.25×10^{-4} m	0.035 m	1.10 m

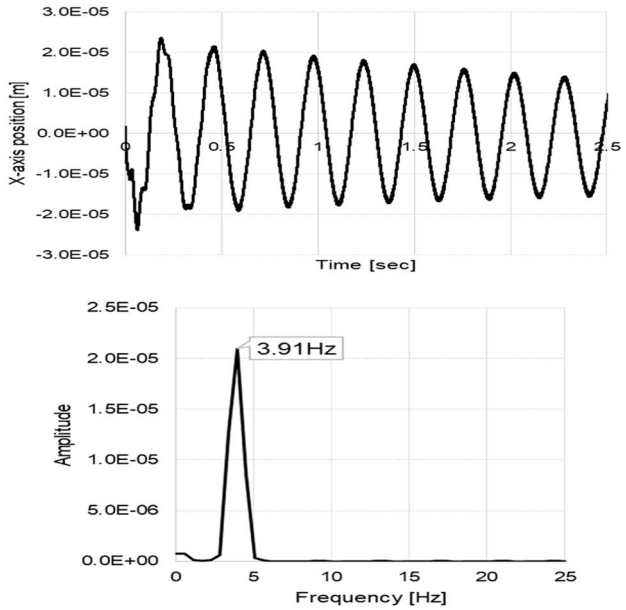

(a) Zero gravity condition

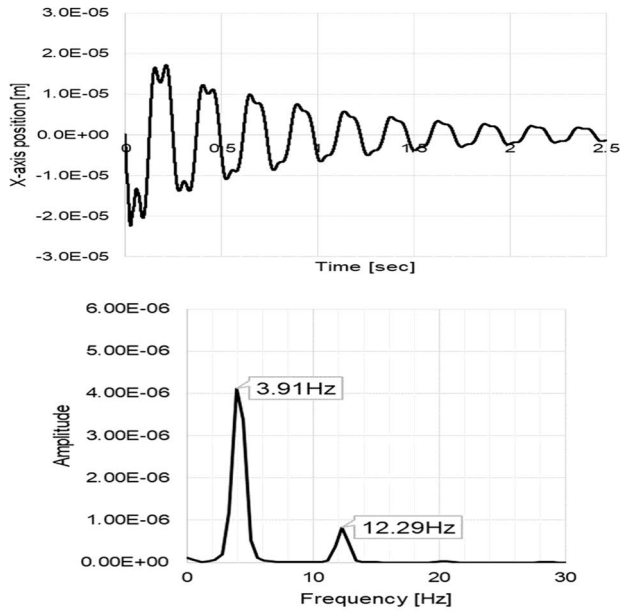

(b) With the proposed control system

Fig. 6 Time history and power spectrum of the displacement in *x*-direction when supported at 22% from the end

reproduced. In more detail, it can be seen that when the proposed control system is used, a small vibration component appeared at around 12.3 Hz. This mode was different from the first mode of free vibration observed in Fig. 6, and was slightly excited in the component of the two-point supporting mode. This was due to the shearing force of the beam at the

Table 3 The property of the panel

Weight	Thickness	Height	Length
2.145 kg	4.5×10^{-2} m	0.92 m	0.46 m

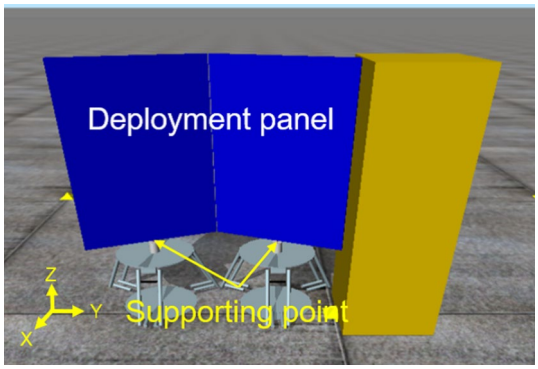

Fig. 7 Demonstration model of deployment structure

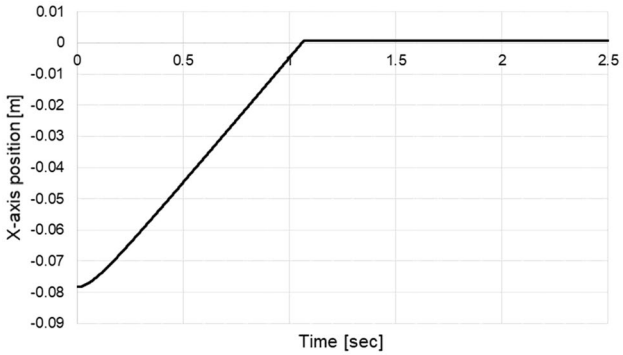

Fig. 8 *X*-directional position of the panel's hinge of the mockup model

supporting point of the robot. The control system of the robot could not completely cancel the reaction force at the supporting point caused by vibration or deployment. This phenomenon was expected to improve in the future by speeding up the response of the robot.

Next, for a demonstration, a numerical simulation of a mockup model of a spacecraft with a deployable solar panel was performed using the proposed control system. Figure 7 shows a simulation model of deployment structure, which has a main body and two panels connected through rotational hinge and spring. Panel properties were given as shown in Table 3.

From Fig. 8, it can be confirmed that using the control system proposed good development is performed without exciting harmful vibration.

6 Hardware experiments

6.1 Simple beam model

At first, the support experiment was conducted with two robots to reconstruct free vibration of the beam, as in the numerical simulation. Figure 9 shows the device experiment. The beam was supported by the two robots at points located 242 mm. The external force was applied at the center of the beam (550 mm).

Figure 10 shows the displacement of the vibration in the direction (x-axis) at the point supported by the left robot after an external force is applied. In comparison with Fig. 6, the hardware experiment exhibited faster damping than the simulation result. But the natural frequency of mode 1 (theoretical value is 4.00 Hz) seems in Figs. 6 and 10 are almost consistent. In the hardware experiment, vibration damping is fast to influence the rolling friction of the jig in the support part. We can see no other vibration mode except the mode 1. The system has no harmful vibration caused by structural oscillation or actuator movement such as the vibration of the harmonic drive gears. Looking at support performance, we can see that can nearly be reconstructed free vibration of the beam in gravity-free space, by the robot system suggested.

Succeeding in the experiments on the uniform beam, we implemented a hardware experiment using a mock-up model as a demonstration.

Figure 11 shows the experimental setup. This set up has deployable solar panel mock-up. Two panels are connected to each other through hinges with springs. The parameters of the panel are the same as Table 3.

Table 4 shows the hardware devices that make up the robotic unit used in this study. The overview of the robot unit is shown in Fig. 12, and system architecture of the hardware robotic unit is summarized in Fig. 13.

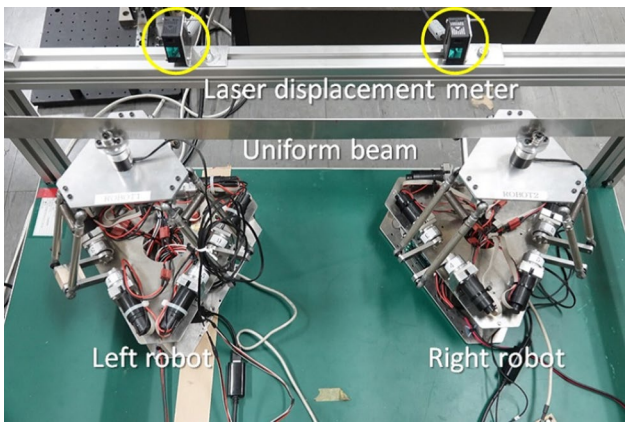

Fig. 9 Experimental setup of a uniform beam model

In the hardware experiment of the mock-up model, the panels are folded from the beginning. At the starting timing, the wire which locked the panel released and the panel began to deploy. The position in the x-axis of the

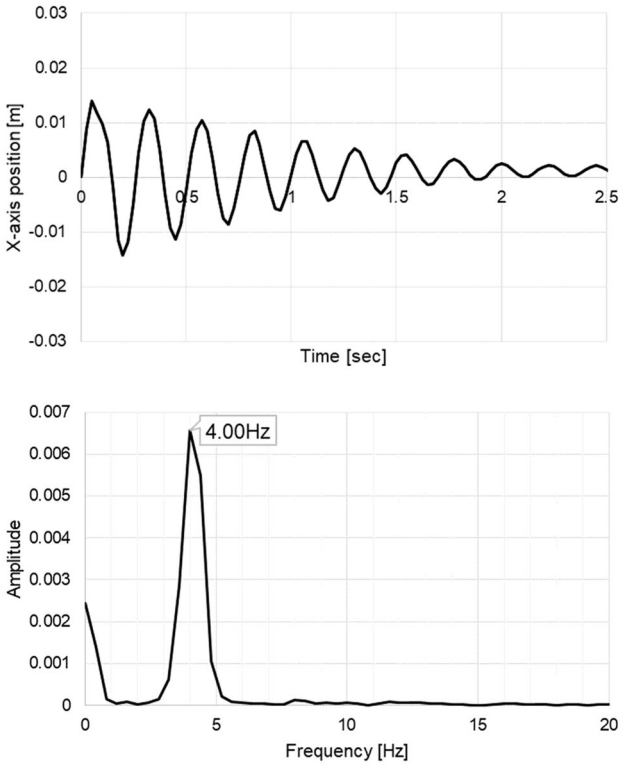

Fig. 10 Time history and power spectrum of the displacement in x-direction when double supported at 22% from the ends

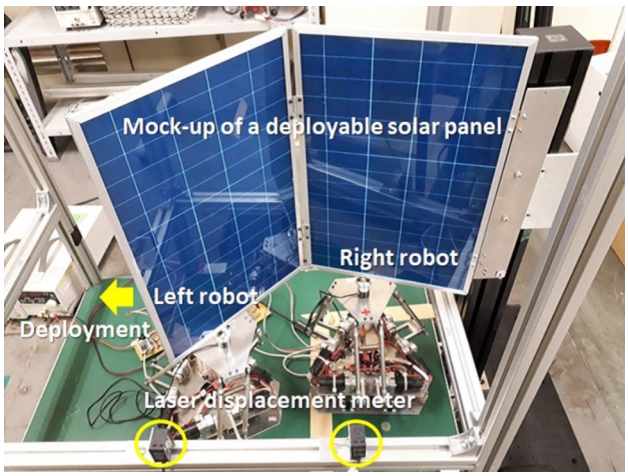

Fig. 11 Experimental setup of a mock-up satellite model. The deployable panels are connected to the fixed pillar at the right side. Two laser displacement meters are mounted to the fixed frame of the experimental field and detect the displacement of the panel in the x-axis

Table 4 Hardware devices

Controller	iMCs01 (iXs Research Co. Ltd)
DC-motor	2642W012C (FAULHABER Co. Ltd.)
Encoder	IE3-512 (FAULHABER Co. Ltd.)
Gears	CSF-8-50-2XH-F-SP (Harmonic drive systems inc.)
Force sensor	USLG25-10N-E (Tec Gihan Co. Ltd.)
Motor driver	Dual MC33926 Motor Driver (Pololu Corporation)

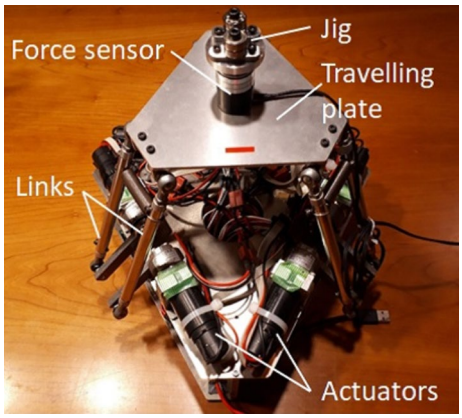

Fig. 12 Hardware system of the robotic unit. The traveling plate is driven by 6 actuators. On the traveling plate, the force sensor is mounted. The supporting jig is at the top of the force sensor

hinge of the panels is measured by the laser displacement meter and recorded. The figure shows the result. From Fig. 14, the robotic unit followed the deployment of the mock-up solar panel without a harmful disturbance or serious oscillation to the system. After the deployment of the panel, there is no harmful vibration on the system, either. We can note that the proposed system effectively support the deployment of the flexible structure in two-directional motion.

7 Conclusions

We proposed and designed a new type gravity compensation system for the prototype test of spacecraft. The system is composed of multi-robotic support units with a simple force controller. From the simulation study, it was noted that assigning the positions of the supporting points to the nodes of the dominant mode of vibration is effective to emulate the free vibration. The validity of the proposed system is verified through hardware mock-up model. For future work, we are thinking about improving the responsiveness of the robot and fusing with the behavior measurement system at the time of development of the deployed structure. In addition, we aim to develop a system that can measure precise transient response characteristics of structures as well as gravity compensation.

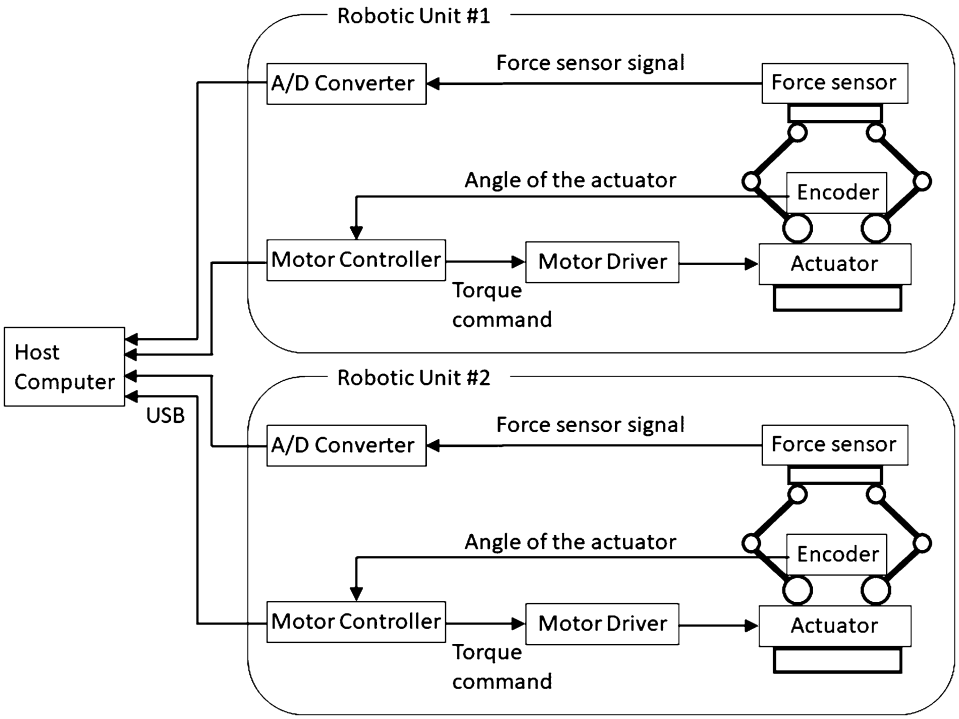

Fig. 13 Architecture of the hardware system

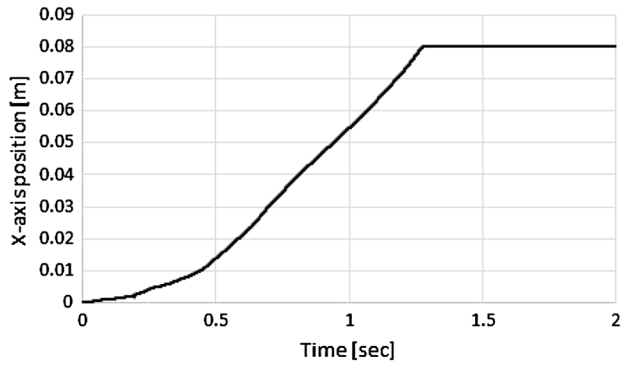

Fig. 14 *X*-directional panel position

Acknowledgements We would like to express my special thanks of gratitude to Dr. Naoko Kishimoto who gave me very important advice and cooperation.

References

1. ”Mars 2020 Rover,” NASA, updated August 4, 2017, https://www.nasa.gov/mars2020. Accessed 10 Nov 2018
2. ”Orion Spacecraft,” NASA, updated March 26, 2019. https://www.nasa.gov/exploration/systems/orion/index.html. Accessed 1 Apr 2019
3. ”Launch schedule, Upcoming Launch Vehicle and Satellite Launches,” JAXA, http://global.jaxa.jp/projects/in_progress.html, updated: October 30, 2018. Accessed 10 Dec 2018
4. Paules G, Luther M (2000) NASA’s Earth science program-increasing science opportunity and payoff through small satellites. Acta Astronaut 46:61–64
5. Esper J, Panetta PV, Ryschkewitsch M, Wiscombe W, Neeck S (2000) NASA-GSFC nano-satellite technology for Earth science missions. Acta Astronaut 46:287–296
6. Fischer A, Pellegrino S (2000) Interaction between gravity compensation suspension system and deployable structure. J. Spacecr Rockets 37:93–99
7. Schultheiß Daniel, ”Gravity Compensation of Deployable Solar Arrays for Small Spacecraft,” http://www-civ.eng.cam.ac.uk/dsl/publications/Schultheiss_Diploma_paper.pdf. Accessed 10 Jan 2019
8. Xu Z, Guannan Y, Hai H, Xinsheng W (2010) Deployment analysis and test of a coilable mast for BUAA Student Micro-satellite, IEEE systems and control in aeronautics and astronautics (ISSCAA), 3rd international symposium, pp 1339–1332
9. Sawada H, Mori O, Okuizumi N, Shirasawa Y, Miyazaki Y, Natori M et al (2011) Mission report on the solar power sail deployment demonstration of IKAROS. In: 52nd AIAA/ASME/ASCE/AHS/ASC structures, structural dynamics and materials conference
10. Greschik G, Mikulas MM (2002) Design study of a square solar sail architecture. J. Spacecr. Rockets 39:653–661
11. Meguro A (1993) A module concept for a cable-mesh deployable antenna. In: 27th aerospace mechanism symposium, NASA-CP-3205, pp 51–66
12. Meguro A, Mitsugi J (1995) Design and analysis of deployable modular mesh structures for a large space antenna. In: 6th European space mechanisms and tribology symposium, ESA-SP-374, pp 319–324
13. Schenk Mark, Viquerat Andrew D, Seffen Keith A, Guest Simon D (2014) Review of inflatable booms for deployable space structures: packing and rigidization. J. Spacecr. Rockets 51:762–778
14. Dean W, Sparks Jr, Juang JN (1992) ’Survey of experiments and experimental fascilities for control of flexible structures. J Guidance Control Dyn 15
15. Sparks DW, Juang J (1992) Survey of experiments and experimental facilities for control of flexible structures. J Guidance Control Dyn 15:801–816
16. Zwanenburg R (1995) The qualification test programme of the ENVISAT solar array mechanism. In: Sixth European space mechanisms and tribology symposium, pp 65–72
17. Engineering Test Satellite VIII ”KIKU No.8” (ETS-VIII), JAXA, 2012. http://global.jaxa.jp/projects/sat/ets8/. Accessed 15 Sep 2018
18. Schwartz Jana L, Peck Mason A, Hall Christopher D (2003) Historical review of air-bearing spacecraft simulators. J Guidance Control Dyn 26:513–522
19. Nitta K, Tsujita K, Kishimoto N (2016) Development of a robotic gravity compensation system for the prototype test of spacecraft. In: IEEE/SICE int. conf. of symposium on system integration, pp 272–277
20. Abe M, Natori MC, Higuchi K, Shiogama Y (1998) Behavior of space membrane at retrieval phase. J Jpn Soc Civ Eng 598(I–44):247–256 (in Japanese)